NANO LETTERS

2008
Vol. 8, No. 8
2447-2451

Synthesis of PbTe Nanowire Arrays using Lithographically Patterned Nanowire Electrodeposition

Y. Yang,† S. C. Kung,† D. K. Taggart,† C. Xiang,† F. Yang,† M. A. Brown,† A. G. Güell,‡ T. J. Kruse,† J. C. Hemminger,† and R. M. Penner*,†

Department of Chemistry and Institute for Surface and Interface Science (ISIS), University of California, Irvine, California 92697-2025, and Department of Physical Chemistry, University of Barcelona, Marti i Franques 1, 08028, Barcelona, Spain

Received May 20, 2008; Revised Manuscript Received June 26, 2008

ABSTRACT

We describe the preparation by electrodeposition of arrays of lead telluride (PbTe) nanowires using the lithographically patterned nanowire electrodeposition (LPNE) method. PbTe nanowires had a rectangular cross-section with adjustable width and height ranging between 60−400 nm (w) and 20−100 nm (h). The characterization of these nanowire arrays using X-ray diffraction, transmission electron microscopy and electron diffraction, scanning electron microscopy, atomic force microscopy, and X-ray photoelectron spectroscopy (XPS) is reported. PbTe nanowires were electrodeposited using a cyclic electrodeposition-stripping technique that produced polycrystalline, stoichiometric, face-centered cubic PbTe with a mean grain diameter of 10−20 nm. These nanowires were more than 1 mm in length and two additional processing steps permitted their suspension across 25 μm air gaps microfabricated on these surfaces. The LPNE synthesis of lithographically patterned PbTe nanowires was carried out in unfiltered laboratory air. Nanowires with lengths of 70−100 μm showed an electrical resistivity comparable to bulk PbTe. XPS reveals that exposure of PbTe nanowires to air causes the formation on the nanowire surface of approximately one monolayer of a mixed lead oxide and tellurium oxide within a few minutes.

Lead telluride is a 0.31 eV (300 °C) bandgap semiconductor that has applications in mid-infrared lasers,[1–3] optical detectors,[4,5] and thermoelectrics.[6–9] Interest in the thermoelectric properties of PbTe nanowires has been heighten by the prediction by Dresselhaus and co-workers[10,11] that the thermoelectric performance, embodied by the dimensionless figure-of-merit (ZT), will increase for wires as the diameter of these wires is reduced to the nanometer scale. In accord with these predictions, enhancements in ZT have been observed for superlattices of 2D quantum wells[12] and very recently for nanowires composed of pure silicon.[13,14]

Nanowires of PbTe and/or other lead chalcogenides have been obtained using a variety of synthetic approaches including (1) the borohydride reduction of Pb^{2+} in the presence of Se to produce PbSe nanowires,[15] (2) precipitation of PbSe nanowires in liquid crystalline media,[16] (3) self-assembly of PbE (E = Se, S, Te) nanotubes from colloids,[17] (4) solvothermal synthesis of PbS nanorods,[18] (5) hydrothermal synthesis of PbTe nanorods and nanotubes,[19,20] (6) vapor−liquid−solid (VLS) synthesis of hyperbranched PbSe nanowires,[21] and (7) chemical vapor transport (CVT) synthesis of PbE (E = Se, S, Te) nanowires.[22] In addition to wires, PbTe nanoparticles,[23] nanoboxes,[24] and nanofilms[25,26] have been reported. With the exception of the films, the product in all these examples is a powder that is disordered in terms of the orientation of the nano-objects. Attaching electrical contacts to these wires, rods, and tubes and/or arranging them into parallel arrays requires the manipulation of these objects, requiring additional and nontrivial processing steps.

A higher degree of organization can be obtained by electrodepositing materials into porous templates that possess oriented pores of a defined and narrowly dispersed diameter.[27] This has proven to be a particularly powerful and versatile method for preparing nanowires of Bi_2Te_3, another small bandgap semiconductor that is closely related to PbTe.[27] Stacy[28–33] and Martin[34] have used template synthesis to prepare cylindrical polycrystalline nanowires with minimum dimensions in the 20−30 nm range and lengths of up to 70 μm.[33] Myung et al.[35] have shown that compositionally modulated nanowires with alternating Bi_2Te_3 and SbTe segments can be prepared by electrodeposition into aluminum oxide templates. Single crystalline nanowires of PbTe have also been obtained using this method.[36] We[37,38] have demonstrated that arrays of Bi_2Te_3 nanowires with diameters as small as 30 nm could be prepared on graphite electrodes using electrochemical step edge decoration (ESED).

* To whom correspondence should be addressed. E-mail: rmpenner@uci.edu.
† University of California.
‡ University of Barcelona.

10.1021/nl801442c CCC: $40.75
Published on Web 07/12/2008

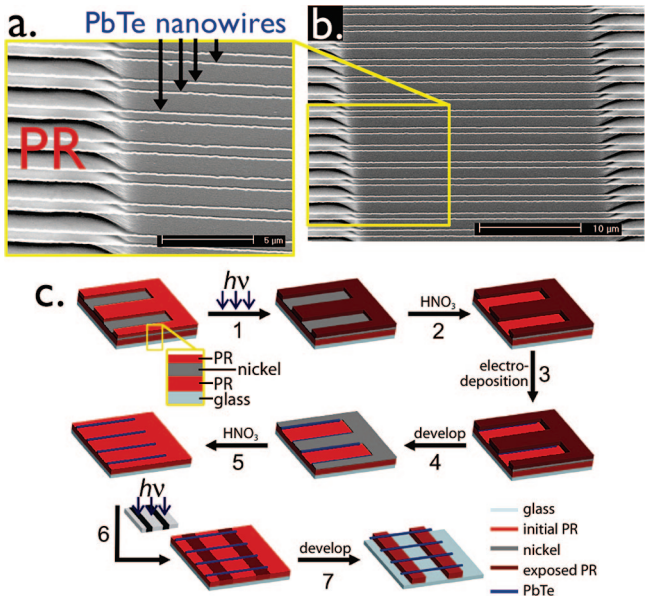

Figure 1. Synthesis of air-suspended PbTe nanowires. (a,b) SEM images of suspended PbTe nanowire arrays at 2 μm pitch density. The air gap between the PbTe nanowires and the glass surface is $\approx$2 μm in this case. (c) Process flow for PB-LPNE commencing, at upper left, with step 4 of the "baseline" LPNE process (Supporting Information, Figure S1). Unique to PB-LPNE is the PR layer interposed between the nickel and glass.

A technique for patterning nanowires of PbTe on the surfaces of dielectrics would simplify their incorporation into circuits. We have been developing a method that involves the fabrication of a sacrificial, horizontal template using conventional microfabrication methods. Our method, called lithographically patterned nanowire electrodeposition (LPNE)[39] uses photolithography to prepare a three-sided "nanoform" into which a nanowire can be electrodeposited using the horizontal nickel edge that defines the back surface of this nanoform. The new method described here, called photoresist-bottomed LPNE or PB-LPNE (Figure 1c), permits air-suspended PbTe nanowires to be fabricated as follows: First, a 1−2 μm thick photoresist (PR) layer (Shipley S1800 series) is spin-coated onto a glass surface. The nanoform architecture is then created atop this photoresist-covered surface as previously described[39] (Supporting Information, Figure S1): A nickel layer was thermally deposited, a positive-tone PR was coated onto this nickel layer and photopatterned, then (Figure 1c, step 1) the sample was irradiated with a UV-lamp to flood-expose the top-photoresist patterns that were not previously exposed/developed. A crucial point is that after this flood-exposure, no developing is carried out. Next (Figure 1c, step 2), the exposed nickel is etched using HNO_3 to produce a 500 nm deep undercut at the edges of the exposed regions. The horizontal trench formed around the perimeter of the exposed region is the nanoform into which the PbTe nanowires will be electrodeposited. The height of this nanoform equals the thickness of the nickel layer which defines the vertical back of the trench. This nanoform follows the contour of the photopatterned region. PbTe nanowire synthesis occurs next (step 3) and is described in detail in the next paragraph. In step 4,

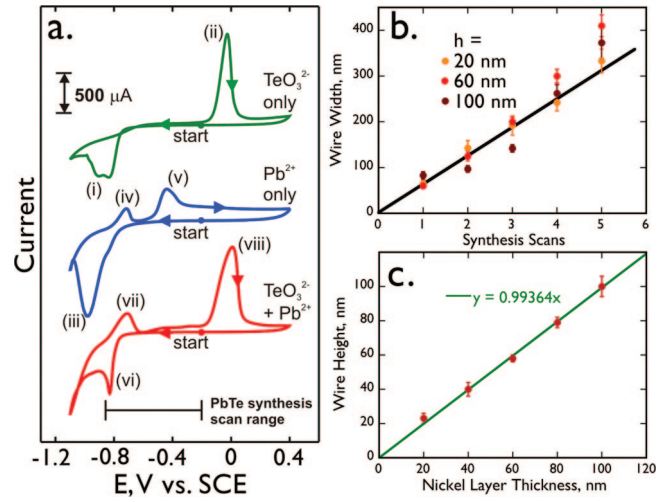

Figure 2. (a) Cyclic voltammograms (50 mV s^{-1}) for deposition of tellurium (top, blue, $[TeO_3^{2-}] = 0.83$ mM), lead (middle, green, $[Pb^{2+}] = 83$ mM) and lead telluride (bottom, red, $[TeO_3^{2-}] = 0.83$ mM and $[Pb^{2+}] = 83$ mM) at pH=10 in aqueous solution. The voltammetric waves labeled in panel a are assigned to the following processes: wave (i), $TeO_3^{2-} + 6H^+ + 4e^- \rightarrow Te(s) + 3H_2O$; wave (ii), $Te(s) + 3H_2O \rightarrow TeO_3^{2-} + 6H^+ + 4e^-$; wave (iii), $Pb^{2+} + 2e^- \rightarrow Pb(s)$; wave (iv), $Pb(s) \rightarrow Pb^{2+} + 2e^-$; wave (v), $Pb(s) + H_2O \rightarrow PbO + 2H^+ + 2e^-$; wave (vi), $Pb^{2+} + TeO_3^{2-} + 3H_2O + 6e^- \rightarrow PbTe(s) + 6OH^-$ and, $Pb^{2+} + 2e^- \rightarrow Pb(s)$; wave (vii), $Pb(s) \rightarrow Pb^{2+} + 2e^-$; wave (viii), $PbTe(s) + 6OH^- \rightarrow Pb^{2+} + TeO_3^{2-} + 3H_2O + 6e^-$. (b) PbTe nanowire width versus the number of synthesis scans employed for electrodeposition. Data are shown for three wire thickness values of 20 (orange), 60 (red), and 100 nm (wine). (c) Relationship of PbTe wire height with thickness of nickel layer.

the (previously exposed) top-PR layer was removed in a developing solution prior to the routine removal of nickel patterns in step 5 leaving free-standing nanowires on top of an intact and unexposed layer of bottom-PR.

The combination of step 1 (exposure) and step 4 (developing), separated across the nanowire-electrodeposition process of steps 2 and 3, is the key for obtaining suspended nanowires in the following steps 6 and 7. The "pre-exposure" of the top PR layer in step 1, at a point where the bottom PR layer is fully shielded from UV illumination by nickel, permits the selective removal of the top PR layer in step 4. Two attributes of this process should be emphasized: First, the suspension of PbTe nanowires involved no dry etching and the associated highly reactive reagents as is typically required to produce suspended structures. Second, all processing steps required for the LPNE synthesis of PbTe nanowires were carried out in an unfiltered laboratory air environment. The minimum nanowire dimension for achieving nanowire suspension across 25 μm gaps without breaking in the final step was in the 40 to 60 nm height range; wires of smaller height were subject to some breakage. Since the critical processing steps occur at a PR coated surface, any rigid surface on which a uniform PR coating can be prepared is suitable for creating suspended nanowires using this approach.

PbTe nanowire synthesis in step 3 is the most important step within this process. We synthesized PbTe using a cyclic electrodeposition-stripping method (Figure 2a) that is similar

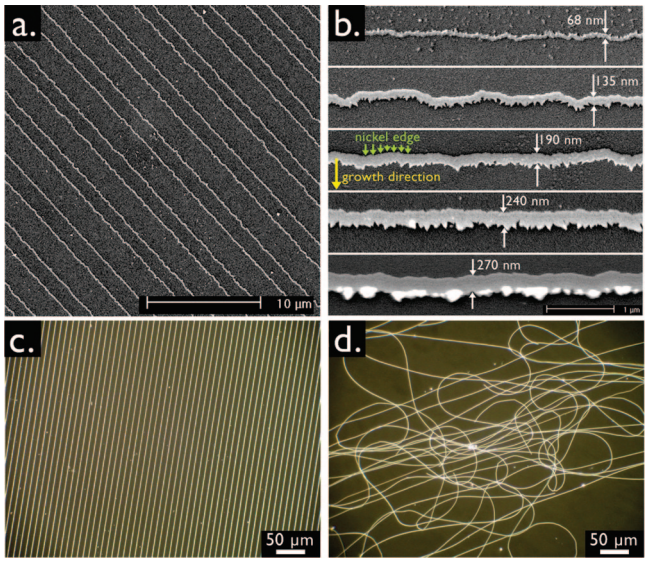

Figure 3. (a) SEM image of a PbTe nanowire array in which the lateral dimensions of the nanowires are 20 nm (h) × 135 nm (w). (b) SEM images of individual PbTe nanowires with thickness = 20 nm and widths of 60−300 nm (from top to bottom). In each of these images, the nickel edge was located at the top edge of the nanowire, and the growth direction was from top to bottom. (c) Optical micrograph of PbTe nanowire arrays of 10 μm lateral pitch. These nanowires had lateral dimensions of 40 nm (h) × 350 nm (w). This image shows millimeter-scale wire lengths and continuity. (d) PbTe wires after release from a glass substrate by turbulent rinsing illustrating the mechanical continuity and strength of these nanomaterials.

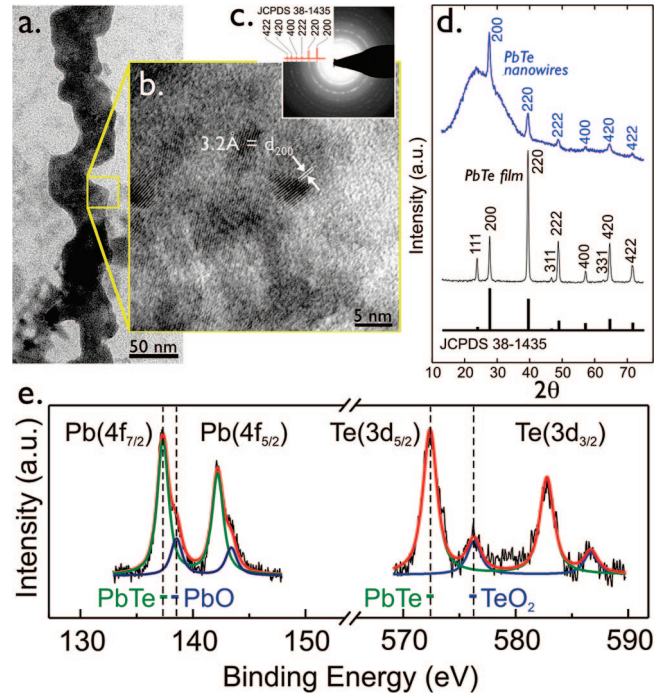

Figure 4. Characterization of PbTe nanowires synthesized by LPNE. (a) TEM image of a PbTe nanowire with dimensions of 20 nm (h) × 45 nm (w). (b) High-resolution TEM image showing lattice fringes spaced by 3.2 Å assignable to the lattice periodicity along [200]. (c) Selected area electron diffraction (SAED) powder pattern for PbTe nanowires showing the assignment of six reflections to fcc PbTe (JCPDS 38−1435). (d) LIXRD patterns for an array of PbTe nanowires with dimensions of 60 nm (h) × 200 nm (w) (blue) and an electrodeposited PbTe film of ≈75 nm in thickness (black). A broad reflection centered at 22° in the XRD pattern for PbTe nanowires (blue curve) is contributed by the glass substrate. A reference XRD stick pattern is shown for fcc PbTe (JCPDS 38−1435). (e) High-resolution X-ray photoelectron spectroscopy spectra of an array of PbTe nanowires showing Pb (4f) and Te (3d) regions. Reference binding energies for PbTe, PbO, and TeO_2 are indicated at bottom.

to the method we described earlier[37,38] for nanowires of Bi_2Te_3. In this method, PbTe and elemental lead were electrodeposited concurrently from a highly asymmetric plating solution containing 83 mM $Pb(NO_3)_2$ and 0.83 mM TeO_2 on the negative-going voltammetric scan to −0.85 V (Figure 2a, wave (vi)). No excess Te is produced on this scan because the concentration of TeO_3^{2-} is 0.01 that of Pb^{2+}. The excess lead was then selectively stripped from the deposit (Figure 2a, wave (vii)). The positive limit of −0.20 V was selected to maximize lead removal without inducing PbTe dissolution (reaction (viii)). Wire width and thickness were controllable without cross-talk over the range from 60−400 nm (width) and 20−100 nm (height by AFM) as shown in Figure 2b,c. As an example, three voltammetric scans generated nanowires 200 ± 10 nm in width and 20 ± 1 nm in vertical height.

If steps 6 and 7 of Figure 1c are omitted, then PbTe wires are obtained on a planar photoresist surface. Such an array, consisting of 20 nm (h) × 135 nm (w) nanowires is shown in the scanning electron microscopy (SEM) image of Figure 3a. High-magnification SEM images of PbTe nanowires of five widths varying from 68 to 270 nm (Figure 3b) reveal several important morphological trends: the edge of the wire that grows in contact with the nickel electrode is smooth while the edge that grows in contact with the plating solution is roughened. The roughness of this wetted edge increases with increasing growth time and wire width. If the horizontal trench is overgrown, the nanowire height is no longer constrained and the PbTe "blooms" at the wetted edge of the nanowire as seen in Figure 3b, bottom image. For the series of nanowires shown in Figure 2b, the horizontal trench had a width of just 250 nm. The optical micrograph of Figure 3c shows an array of PbTe wires that are 40 nm (h) × 350 nm (w) and millimeters in total length. The mechanical continuity of these nanowires is readily demonstrated by releasing them from the photoresist surface by dissolving it using acetone (Figure 3d).

A PbTe nanowire 40−45 nm in width and 20 nm in height is shown in the transmission electron microscope image of Figure 4a. Lattice fringes separated by 3.2 Å (Figure 4b) are consistent with the periodicity along [200]. Selective-area electron diffraction (Figure 4c) produces a powder pattern in which six reflections can be indexed to face-centered cubic (fcc) PbTe (JCPDS 38−1435). X-ray diffraction patterns were acquired for PbTe arrays, deposited at 2 μm pitch, by utilizing low-angle incidence (0.3°) X-ray diffraction (LIXRD)[40,41] (Figure 4d, top) in which the incident angle is below the critical angle. The broad peak centered at $2\theta = 25°$ derives from reflections from the photoresist surface. Six reflections superimposed on this background can be assigned to fcc PbTe (JCPDS 38−1435), and Scherrer

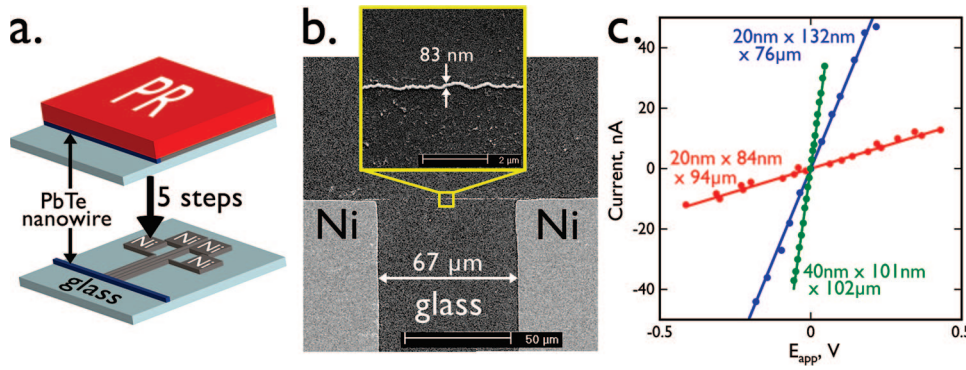

Figure 5. (a) Schematic showing that the patterned nickel edge used for nanowire growth can later be patterned and used for a four-point electrical measurement of the wire resistance. (b) SEM image of the inner two nickel electrodes and a PbTe nanowire. The electrically isolated wire length in this instance was 94 μm, greater than the interelectrode distance of 67 μm. (c) Ohmic current versus voltage plots for three PbTe nanowires with dimensions as indicated. The conductivities derived from these data are listed in Table 1.

analysis of these linewidths yields a grain diameter of 10−20 nm. For purposes of comparison, we also carried out the synthesis of thin PbTe films on nickel-coated glass (Figure 4d, middle). Such films show a preferred growth direction of [220] but this orientational preference is not detected for nanowire growth at nickel edges. Neither the nanowires nor the film show reflections other than those assignable to cubic PbTe suggesting that these materials are single phase.

The chemical state of the nanowire surface is a critically important issue that is not addressed by XRD. We carried out an X-ray photoelectron spectroscopy (XPS) study of PbTe nanowire arrays aimed at discovering the presence of oxides on these surfaces (Figure 4e). Two groups of peaks at 137.3 and 142.2 eV are assigned to Pb($4f_{7/2}$) and Pb($4f_{5/2}$), respectively. Each group contains a shoulder peak on the high binding energy side. Deconvolution curve fitting distinguishes two components at 137.3 and 138.5 eV, corresponding to the expected chemical shifts for PbTe[42] and either $Pb(OH)_2$[43] or PbO,[44] respectively. The ratio of $Pb(O)_x$/PbTe is ≈0.27. Likewise, the envelope for Te(3d) can be deconvoluted into two components that we assign to PbTe and TeO_2.[45] The ratio of TeO_2/PbTe is ≈0.23. On the basis of the layered oxide structure model suggested by Bando et al.[46] and the inelastic mean free paths of the photoelectrons,[47] we estimate that within a few minutes of air exposure, the oxide, on the freshly prepared nanowires, consists of a mixed oxide layer equivalent to pure layers of PbO (thickness = 0.56 nm) and TeO_2 (0.37 nm). This equates to approximately one monolayer of the mixed oxide.

The electrical resistance of single PbTe nanowires was measured by microfabricating a four point nickel contact from the same nickel layer used in the LPNE process (Figure 5a). Because the PbTe nanowire grows in intimate electrical contact to this nickel surface, using the nickel edge as an electrical contact prevents the formation of an insulating oxide layer on the nanowire surface prior to the application of the electrical contact. The electrically isolated length of the PbTe nanowire was between 76 and 102 μm (Figure 5b). Current versus voltage plots were ohmic for these nanowires, corresponding to electrical conductivities of between 0.70 × 10^4 and 1.8 × 10^4 S/m; this is within the range of conductivity values reported for bulk PbTe previously.[48,49,22]

Table 1. Conductivity of PbTe Derived from Resistance Measurements on Single PbTe Nanowires and Comparison with Literature Values for Bulk PbTe

wire dimensions	height (nm)	width (nm)	length (μm)	σ (10^4 S/m)
sample 1	40 (±2)	101 (±8)	102	1.81 (±0.09)
sample 2	20 (±2)	132 (±9)	76	0.70 (±0.06)
sample 3	20 (±2)	84 (±4)	94	0.19 (±0.01)
ref 48				0.5−5
ref 49				1
ref 22				0.1

In summary, stoichiometric and single phase PbTe nanowire arrays have been prepared using a new method, PB-LPNE, that provides for control over wire width and thickness, photolithographic patterning, and the suspension of nanowires across 25 μm air gaps separating photoresist supports. The resulting nanowire-substrate system provides new opportunitities for the investigation of optical, electrical, and thermoelectric properties.

Acknowledgment. This work was supported by NSF DMR-0654055 (R.M.P.), the DOE Office of Basic Energy Sciences DE-FG02-96ER45576 (J.C.H.), and the UCI School of Physical Sciences Center for Solar Energy (R.M.P. and J.C.H.). A.G.G. gratefully acknowledges economical support from the Department of Universities, Research, and Information Society (DURSI) of the Catalonia Government through Grant 2007-BE-1-00232.

Supporting Information Available: This material is available free of charge via the Internet at http://pubs.acs.org.

References

(1) Springholz, G.; Schwarzl, T.; Aigle, M.; Pascher, H.; Heiss, W. *Appl. Phys. Lett.* **2000**, *76*, 1807–1809.
(2) Schwarzl, T.; Heiss, W.; Springholz, G.; Aigle, M.; Pascher, H. *Electron. Lett.* **2000**, *36*, 322–324.
(3) Sze, S. M.; Ng, K. K. *Physics of semiconductor devices*, 3rd ed.; Wiley-Interscience: Hoboken, NJ, 2007.
(4) Boschetti, C.; Bandeira, I.; Closs, H.; Ueta, A.; Rappl, P.; Motisuke, P.; Abramof, E. *Infrared Phys. Technol.* **2001**, *42*, 91–99.
(5) Barros, A.; Abramof, E.; Rappl, P. *J. Appl. Phys.* **2006**, *99*, 024904.
(6) Rowe, D. M. *CRC Handbook of Thermoelectrics*; CRC Press: Boca Raton, FL, 1995.
(7) Dughaish, Z. *Physica B-Condensed Matter* **2002**, *322*, 205–223.
(8) Heremans, J.; Thrush, C.; Morelli, D. *Phys. Rev. B* **2004**, *70*, 115334.
(9) Heremans, J.; Thrush, C.; Morelli, D. *J. Appl. Phys.* **2005**, *98*, 063703.

(10) Hicks, L.; Dresselhaus, M. *Phys. Rev. B* **1993**, *47*, 16631–16634.
(11) Lin, Y.; Sun, X.; Dresselhaus, M. *Phys. Rev. B* **2000**, *62*, 4610–4623.
(12) Venkatasubramanian, R.; Siivola, E.; Colpitts, T.; O'Quinn, B. *Nature* **2001**, *413*, 597–602.
(13) Boukai, A. I.; Bunimovich, Y.; Tahir-Kheli, J.; Yu, J.-K.; Goddard, W. A. I.; Heath, J. R. *Nature* **2008**, *451*, 168–171.
(14) Hochbaum, A. I.; Chen, R.; Delgado, R. D.; Liang, W.; Garnett, E. C.; Najarian, M.; Majumdar, A.; Yang, P. *Nature* **2008**, *451*, 163–167.
(15) Wang, W.; Geng, Y.; Qian, Y.; Ji, M.; Liu, X. *Adv. Mater.* **1998**, *10*, 1479–1481.
(16) Liu, Y.; Cao, J.; Zeng, J.; Li, C.; Qian, Y.; Zhang, S. *Eur. J. Inorg. Chem.* **2003**, 644–647.
(17) Tong, H.; Zhu, Y.-J.; Yang, L.-X.; Li, L.; Zhang, L. *Angew. Chem., Int. Ed.* **2006**, *45*, 7739–7742.
(18) Zhang, C.; Kang, Z.; Shen, E.; Wang, E.; Gao, L.; Luo, F.; Tian, C.; Wang, C.; Lan, Y.; Li, J.; Cao, X. *J. Phys. Chem. B* **2006**, *110*, 184–189.
(19) Zhang, L.; Yu, J.; Mo, M.; Wu, L.; Kwong, K.; Li, Q. *Small* **2005**, *1*, 349–354.
(20) Sima, M.; Enculescu, I.; Sima, M.; Vasile, E. *J. Optoelectron. Adv. Mater.* **2007**, *9*, 1551–1554.
(21) Zhu, J.; Peng, H.; Chan, C. K.; Jarausch, K.; Zhang, X. F.; Cui, Y. *Nano Lett.* **2007**, *7*, 1095–1099.
(22) Fardy, M.; Hochbaum, A. I.; Goldberger, J.; Zhang, M. M.; Yang, P. *Adv. Mater.* **2007**, *19*, 3047–3051.
(23) Mokari, T.; Zhang, M.; Yang, P. *J. Am. Chem. Soc.* **2007**, *129*, 9864–9865.
(24) Wang, W.; Poudel, B.; Wang, D.; Ren, Z. *Adv. Mater.* **2005**, *17*, 2110–2114.
(25) Saloniemi, H.; Kanniainen, T.; Ritala, M.; Leskela, M. *Thin Solid Films* **1998**, *326*, 78–82.
(26) Saloniemi, H.; Kemell, M.; Ritala, P.; Leskela, M. *J. Electroanal. Chem.* **2000**, *482*, 139–148.
(27) Martin, C. *Science* **1994**, *266*, 1961–1966.
(28) Prieto, A.; Sander, M.; Martin-Gonzalez, M.; Gronsky, R.; Sands, T.; Stacy, A. *J. Am. Chem. Soc.* **2001**, *123*, 7160–7161.
(29) Martin-Gonzalez, M.; Prieto, A.; Gronsky, R.; Sands, T.; Stacy, A. *J. Electrochem. Soc.* **2002**, *149*, C546−C554.
(30) Sander, M.; Gronsky, R.; Sands, T.; Stacy, A. *Chem. Mater.* **2003**, *15*, 335–339.
(31) Prieto, A.; Martin-Gonzalez, M.; Keyani, J.; Gronsky, R.; Sands, T.; Stacy, A. *J. Am. Chem. Soc.* **2003**, *125*, 2388–2389.
(32) Martin-Gonzalez, M.; Snyder, G.; Prieto, A.; Gronsky, R.; Sands, T.; Stacy, A. *Nano Lett.* **2003**, *3*, 973–977.
(33) Trahey, L.; Becker, C. R.; Stacy, A. M. *Nano Lett.* **2007**, *7*, 2535–2539.
(34) Sapp, S.; Lakshmi, B.; Martin, C. *Adv. Mater.* **1999**, *11*, 402–404.
(35) Yoo, B.; Xiao, F.; Bozhilov, K. N.; Herman, J.; Ryan, M. A.; Myung, N. V. *Adv. Mater.* **2007**, *19*, 296–299.
(36) Liu, W.; Cai, W.; Yao, L. *Chem. Lett.* **2007**, *36*, 1362–1363.
(37) Menke, E. J.; Li, Q.; Penner, R. M. *Nano Lett.* **2004**, *4*, 2009–2014.
(38) Menke, E. J.; Brown, M. A.; Li, Q.; Hemminger, J. C.; Penner, R. M. *Langmuir* **2006**, *22*, 10564–10574.
(39) Menke, E. J.; Thompson, M. A.; Xiang, C.; Yang, L. C.; Penner, R. M. *Nat. Mater.* **2006**, *5*, 914–919.
(40) Bontempi, E.; Colombi, P.; Depero, L.; Cartechini, L.; Presciutti, F.; Brunetti, B.; Sgamellotti, A. *Appl. Phys. A* **2006**, *83*, 543–546.
(41) Marra, W.; Eisenberger, P.; Cho, A. *J. Appl. Phys.* **1979**, *50*, 6927–6933.
(42) Pederson, L. *J. Electron Spectrosc. Relat. Phenom.* **1982**, *28*, 203–209.
(43) Taylor, J.; Perry, D. *J. Vac. Sci. Technol., A* **1984**, *2*, 771–774.
(44) Nefedov, V. *Surf. Interface Anal.* **1980**, *2*, 171–175.
(45) Ricco, A.; White, H.; Wrighton, M. *J. Vac. Sci. Technol., A* **1984**, *2*, 910–915.
(46) Bando, H.; Koizumi, K.; Oikawa, Y.; Daikohara, K.; Kulbachinskii, V.; Ozaki, H. *J. Phys.: Condens. Matter* **2000**, *12*, 5607–5616.
(47) Wagner, C.; Naumkin, A.; Kraut-Vass, A.; Allison, J.; Powell, C.; Rumble, J. J. *NIST X-ray Photoelectron Spectroscopy Database*.
(48) Lide, D. R. *CRC Handbook of Chemistry and Physics*; 88th Edition; CRC Press: Taylor & Francis Group, NY, 2007−2008.
(49) Rogacheva, E.; Krivulkin, I.; Nashchekina, O.; Sipatov, A.; Volobuev, V.; Dresselhaus, M. *Appl. Phys. Lett.* **2001**, *78*, 1661–1663.

NL801442C